

Aharonov–Bohm oscillations and equilibrium current distributions in open quantum dot and in ring interferometer

Olga A. Tkachenko¹, Dmitry G. Baksheev², Vitaly A. Tkachenko^{1,2}

¹ Rzhanov Institute of Semiconductor Physics, Siberian Branch, Russian Academy of Sciences, 13 Akad. Lavrent'eva Ave., Novosibirsk, 630090, Russia
² Novosibirsk State University, 1 Pirogova Str., Novosibirsk, 630090, Russia

Corresponding author: Vitaly A. Tkachenko (vtkach@isp.nsc.ru)

Received 26 December 2019 ♦ Accepted 28 April 2020 ♦ Published 30 June 2020

Citation: Tkachenko OA, Baksheev DG, Tkachenko VA (2020) Aharonov–Bohm oscillations and equilibrium current distributions in open quantum dot and in ring interferometer. *Modern Electronic Materials* 6(2): 59–64. <https://doi.org/10.3897/j.moem.6.2.58576>

Abstract

Magnetotransport in two submicron-sized devices formed on the basis of GaAs/AlGaAs structures has been simulated using nonequilibrium Green functions. The effect of a perpendicular magnetic field on quantum transport in a quasi-one-dimensional quantum dot and in an Aharonov–Bohm interferometer has been analyzed in a single-particle approximation. Magnetic field oscillations of two-terminal conductance of the devices, equilibrium (persistent) current distributions and magnetic moment generated in the devices by persistent currents have been determined using numerical methods. Correlations between the magnetic moment, magnetic field oscillations of conductance and energy resonance in a specific magnetic field have been traced. Sufficiently regular conductance oscillations similar to Aharonov–Bohm ones have been revealed for a quasi-one-dimensional quantum dot at small magnetic fields (0.05–0.4 T). For a ring interferometer the contribution to the total equilibrium current and magnetic moment at a specific energy may change abruptly both in magnitude and in sign as a result of changing magnetic field within one Aharonov–Bohm oscillation. We show that the conductance of an interferometer is determined not by the number of modes propagating in the ring but rather by the effect of triangular quantum dots at the ring entrance that produce a strong reflection. The period of the calculated Aharonov–Bohm oscillations is in agreement with the measurement results for these devices.

Keywords

ballistic quantum dot, ring electron interferometer, conductance, equilibrium current, magnetic moment, Aharonov–Bohm oscillations.

1. Introduction

Flexibly controlled submicron devices formed on the basis of high-mobility 2D electron gas and GaAs/AlGaAs heterostructures have been the main object of experimental quantum nanophysics. For example, one-particle interference phenomena in the conductance G are most often studied in small open ballistic

nanosystems in the form of a ring or a quantum dot [1–3] connected with 2D reservoirs via two narrow entrances. The conductance of a nanosized device is defined as $G = I/V$, where I is the nonequilibrium current generated by the small voltage V between the electron reservoirs.

Measurement of Aharonov–Bohm oscillations in the conductance G with variations of a perpendicular mag-

netic field B is a method of estimating the effective area S of devices. The area S is usually evaluated using the following formula suggested by simple one-dimensional models of ring and edge current states: $S = \Phi_0 / \Delta B$, where ΔB is the period of the Aharonov–Bohm oscillations and $\Phi_0 = h/e$ is the magnetic flux quantum. For $\sim 1 \mu\text{m}$ rings in 2D electron gas this evaluation is in a good agreement with the electron microscopic image of the etched-off areas or metallic gate systems forming the electronic nano-system in a real solid state device [1]. However the applicability of this formula has not been verified for quantum dots at small B when the edge current states have not been formed yet. The magnetic field oscillations in this mode are less regular for dots [2, 3] than for rings. Nevertheless the high quality of submicron rings and quantum dots in the 2D electron gas of GaAs/AlGaAs heterostructures provide the possibility to use a realistic simulation for associating data on the 3D structure of the devices with the observed conductance behavior [4–6].

Two examples are quite illustrative in this respect. One of them is the Aharonov–Bohm interferometer with an effective ring diameter of $0.7 \mu\text{m}$ created at the Institute for Semiconductor Physics of the Siberian Branch of the Russian Academy of Sciences by electron lithography and reactive ion etching [7–9]. The other is the open quantum dot with a size of approx. $0.7 \mu\text{m}$ created at the Cavendish Laboratory, UK, using a three-layered system of submicron and ultrathin (60 nm) metallic gates [10–14]. To create these devices the ISP SB RAS and the Cavendish Laboratory have improved the parameters of GaAs/AlGaAs heterostructure molecular beam epitaxy process and obtained 2D electron gas with a low-temperature mobility of 0.5×10^6 and $2.5 \times 10^6 \text{ cm}^2/(\text{V} \times \text{s})$, respectively. In these cases the researchers had a basis for realistic simulation in the form of detailed information on the main specific features of solid state device technologies (materials composition, layer thicknesses and 3D geometry). Comparatively large dimensions of these devices ($0.7 \mu\text{m}$) combined with the high quality of the 2D electron gas and nanolithography allowed ignoring the disorder in the first approximation. The self-consistent solution of the 3D electrostatics problem provided for close-to-real simple forms of effective 2D potential $U(x,y)$ that can be used for calculating the conductance of the devices in a zero magnetic field [7, 12–14]. The calculated potential $U(x,y)$ for these structures is symmetrical relative to the lines $x = 0$ and $y = 0$ (see figs 1, 2 [7], fig. 1 [12] and figs 4–6 [13]). The $0.7 \mu\text{m}$ diameter ring interferometer in question has an axial symmetry except for the small ($0.2 \mu\text{m}$) regions at the connections between the 100 nm wide ring channel and the supplying quantum wires having the same width. The electrostatic potential of the modeled quantum dot has a very simple form unlike the potentials of other quantum dots because it allows separating the variables x and y when solving the quantum scattering problem in a zero magnetic field. Calculations of $U(x,y)$ and simulation of the measured gate characteristics [7] led to the discovery of triangular quantum dots at the entrance and exit of

the ballistic ring, and it was found [12–14] that the earlier reported quantum dot [10, 11] is quasi-one-dimensional, i.e., intersubband scattering is suppressed there in contrast to the typical ballistic quantum dots. These discoveries allowed one to explain the unusual physical phenomena that were observed experimentally.

However the magnetotransport properties have not yet been calculated for these two devices. These properties include the magnetic field oscillations of two-terminal conductance G as well as the distributions of equilibrium (persistent) current which is not accompanied by energy dissipation at any allowed energies below the common Fermi level. These closed-loop currents are induced by an external magnetic field in any electrically conducting systems (including contactless ones) of arbitrary size and dimensions and are in thermodynamic equilibrium. Theoretical analysis of equilibrium currents in a perpendicular magnetic field has only been carried out for some ideal shapes of lateral potential in quantum dots and rings, and mainly for closed systems [15–22]. This was sufficient for understanding the first measurement results for persistent currents. In an experiment these currents can only manifest themselves in an integral parameter, i.e., magnetization or magnetic moment M . The magnetic fields induced by the persistent currents are only a small addition to the external magnetic field. There are few reported measurements of induced magnetic moment in submicron-sized semiconductor rings and quantum dots [23–25] because magnetization measurements even for 2D electron gas [26, 27] are much more complex task than for 3D macroscopic homogeneous semiconductors. In the latter materials magnetic moment oscillations are well known as the de Haas – van Alphen effect.

The aim of this work is to complement realistic simulations for the examples of the ring and the quantum dot not only with a calculation of magnetic field conductance oscillations but also with a calculation of persistent currents and magnetic moment. The calculated conductance oscillations can be compared with earlier measured ones and the calculation of equilibrium currents and the respective magnetic moment is necessary for understanding quantum phenomena and evaluating the prospects for new experiments.

2. Simulation method

The total equilibrium current for the preset Fermi energies E_F and B is determined as the sum of the contributions $d\mathbf{J}(x,y)/dE$ for multiple states with the energies $E \leq E_F$. To calculate $d\mathbf{J}(x,y)/dE$, the nonequilibrium current $\mathbf{I}(x,y)$ and the conductance we used an earlier reported algorithm [28]. The total magnetic moment is calculated as the vector product of the vector radius $\mathbf{r} = (x,y)$ and the current $\mathbf{M} = 0.5\mathbf{r} \times \mathbf{J}(x,y)$. Usually the equilibrium current is studied theoretically and numerically for closed systems with a discrete E_i spectrum [15–22] but we analyze open submicron systems with a continuous spectrum

that are connected to electron reservoirs via permeable smooth potential barriers [4–14]. Note that the method of nonequilibrium Green functions briefly described earlier [28] is ideally suited for the simulation of open systems because the definition of the Green function contains a small imaginary addition to the energy, and not only resonances but also deep energy levels are expressed in the density of states as finite-width E peaks. Out of open systems we have chosen for simulation the close-to-ideal geometries of the ring interferometer and the quantum dot which were studied experimentally and theoretically earlier [7–14]. First of all based on the data on the structures of these devices we calculated the 3D electrostatic potential and effective confining potential $U(x,y)$ in the 2D electron gas. Then, based on the calculated $U(x,y)$ and given B we determined the total nonequilibrium current I through the devices at given E_F and bias voltage V (conductance $G = I/V$) [7, 12–14]. In this work we calculated the $G(B)$ dependences, the $d\mathbf{J}(x,y)/dE$ distributions and the dM/dE contributions to the total magnetic moment M for the states with the given energy E .

3. Quantum dot: Results and discussion

Figures 1–4 show computation results for the quasi-one-dimensional quantum dot. It can be seen from the $G(B)$ dependence (Fig. 1) calculated for the energy at Fermi level $E_F = 0.1$ meV that sufficiently regular oscillations cover the range from 0.05 to 0.4 T. Note that experiments with this quantum dot detected Aharonov–Bohm oscillations with the period $\Delta B = 15$ mT [10] which allowed us to evaluate the area of the electron system of the quantum dot using the following simple formula: $S = \Phi_0/\Delta B$. When comparing with the experimental Aharonov–Bohm oscillations we smoothed down the oscillations in the calculated $G(B)$ function. The oscillations on the smoothed curve $\Delta G_{\text{smooth}}(B)$ have a period of 19 mT. The absence of a strict regularity of the peak sequence in the original $G(B)$ curve is accounted for by the effect of the magnetic field on the quasidecrete energy levels of the quasi-one-dimensional quantum dot.

The peaks in the $G(B)$ function match with narrow positive or negative spikes of dM/dE . The regions of the supplying channels were ignored during the calculation of dM/dE and M .

The calculated equilibrium current pattern in the quasi-one-dimensional quantum dot for a resonance peak in a moderate magnetic field with $B = 0.3345$ T (Fig. 2) provides a vision of the shape of the open dot including the entrance bottlenecks between the dot and the regions of the supplying electron reservoirs (see $U(x,y)$, Fig. 1 [12]). Note that the period of the magnetic field oscillations of the conductance corresponds to the effective area $S = \Phi_0/\Delta B$ which is somewhat smaller than the area of the quantum dot. This is true not only for the calculated

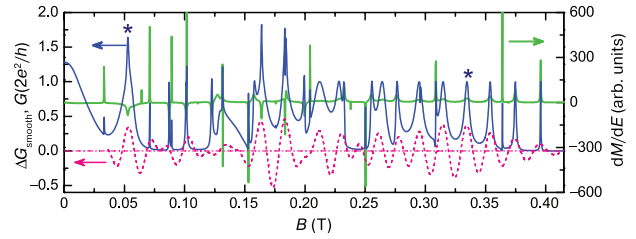


Figure 1. The calculated magnetic field characteristics of the quasi-one-dimensional quantum dot at $E_F = 0.1$ meV: the dependences of the conductance and the derivative of the magnetic moment dM/dE on B . The states clarified in Figs 2–4 are marked with an asterisk. The lower curve is the result of band-pass filtering of $G(B)$.

$\Delta B = 19$ mT as shown by dashed oval in Fig. 2 but also for the experimental one $\Delta B = 15$ mT. The main current flow occurs inside the reservoirs and via the wide ring at the quantum dot periphery. The formal electron path covering the effective area S is equidistant from the internal and external boundaries of the calculated equilibrium current ring at $B = 0.3345$ T.

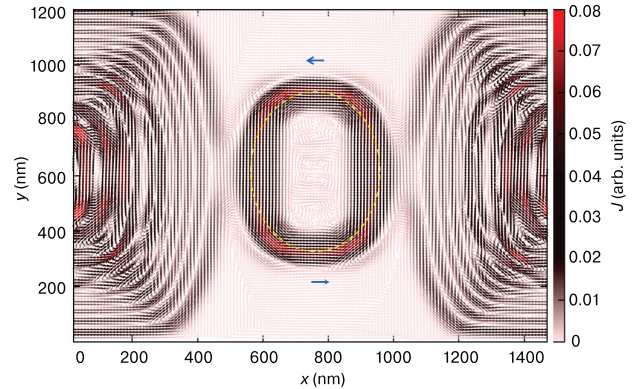


Figure 2. Distribution of total equilibrium current \mathbf{J} in the quantum dot and in the channels at $B = 0.3345$ T. The arrows indicate the direction of the current. The yellow dotted line encircles the effective area S .

The $\sim 200 \times 400$ nm² region in the center of the dot is almost free from currents. On the contrary for the resonance $G(B)$ peak in a weak magnetic field $B = 0.053$ T the equilibrium current J at the same E_F concentrates near the quantum dot center (Fig. 3) and is so high that the current in the electron reservoirs is almost irresolvable against it.

Note that the equilibrium current in the quantum dot in Figs 3, 2 is directed clockwise and counterclockwise, respectively. These fundamentally different patterns of the total equilibrium current J and additional calculations of the $d\mathbf{J}(x,y)/dE$ distributions show that an isolation region associated with the formation of edge current states emerges inside the quantum dot at elevated B but this region is absent at low B . We consider this to be the origin of the noticeable difference in the regularity of the $G(B)$ oscillations in Fig. 1 at the sections (0, 0.2 T) and (0.2, 0.4 T).

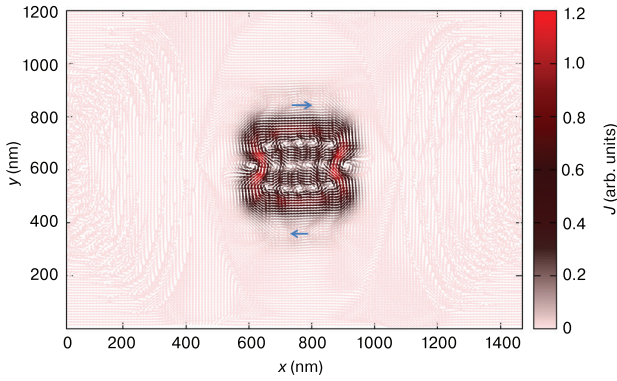


Figure 3. The total equilibrium current \mathbf{J} at the quantum dot at $B = 53$ mT. The arrows indicate the direction of the current.

The equilibrium current $\mathbf{J}(x,y)$ was calculated for the energy range from $E = -3$ meV (potential at the center of the quantum dot) to $E_F = 0.1$ meV but the determinant contribution to the total magnetic moment is made by some resonance states located near the Fermi level and corresponding to $G(E)$ peaks in Fig. 4.

One can see three of these states for $B = 0.3345$ T in Fig. 4a, and they together provide for a positive value of the total magnetic moment M at $E_F = 0.1$ meV which corresponds to the counterclockwise direction of the total equilibrium current J in the quantum dot in Fig. 2. On the contrary for $B = 0.053$ T one dominating state at $E = -0.77$ meV provides for a large by absolute value and negative total magnetic moment M at $E_F = 0.1$ meV (Fig. 4b) which corresponds to the clockwise direction of the current J in the quantum dot in Fig. 3.

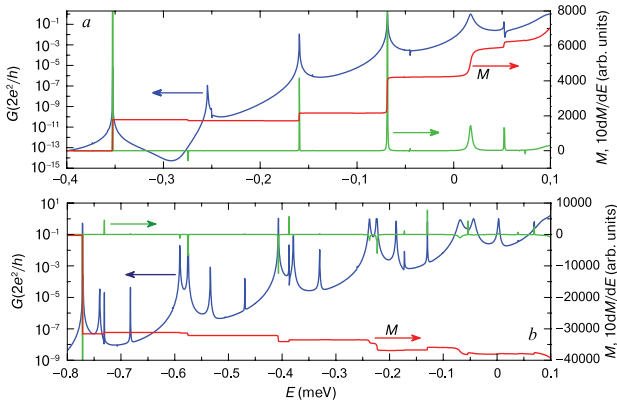


Figure 4. Dependences of the electron transmission coefficient $G(E)$, magnetic moment $M(E)$, and $10dM(E)/dE$ for the quasi-one-dimensional quantum dot in the cases $B = 0.3345$ T (a) and $B = 0.053$ T (b).

Note the regularity of the positions of the main and additional (narrow) peaks in the conductance vs total electron energy function $G(E)$ (Fig. 4). The almost self-repeating sequence of these peaks with an increase in E at a constant B is because the quantum dot is quasi-one-dimensional, that is, electron movement along the x and y axes at $B = 0$ are separable (see figs 7–10 [13] and figs 1, 2 [14]).

4. Ring: Results and discussion

Figure 5 shows the calculated magnetic field oscillations of conductance at the Fermi level and the calculated dM/dE as a function of B for the ring interferometer as described earlier [7–9]. It can be seen that the Aharonov–Bohm oscillations are more homogeneous in this case than for the quantum dot. The oscillation frequency doubles in the 0.07 to 0.12 T range at a constant E , i.e., the twin conductance peaks are split stronger than in the $B = 0$ to 0.06 T range. Note that frequency doubling was already observed experimentally but it was caused by Fermi energy variation [8] rather than by magnetic field variation. The measured oscillations have smaller amplitudes and are smoother than the calculated ones. Their pattern is roughly the same as in the smoothed $\Delta G_{\text{smooth}}(B)$ curve. The period of the calculated Aharonov–Bohm oscillations agrees well with earlier measurement data [8, 9]. Calculations of the potential and the transverse quantization levels in the ring branches and in the supplying quantum wires [7] shows that three electron wave modes may propagate in each of these channels at the Fermi level ($E_F = 0$). However the calculated conductance of the device is only slightly more than unity, just like in the earlier measurements [8, 9] (Fig. 5). This conductance suppression is accounted for by the existence of triangular quantum dots at connections between the ring and the supplying quantum wires and the strong electron wave backscattering at these dots [7].

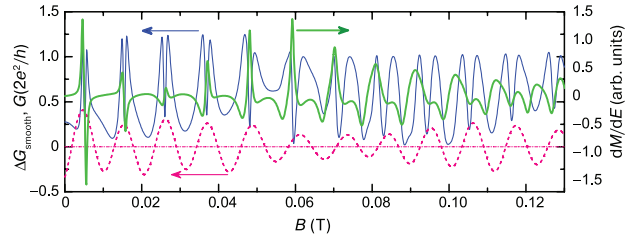


Figure 5. The calculated magnetic field characteristics of the ring interferometer at the Fermi level ($E = 0$): conductance oscillations and derivative of the magnetic moment dM/dE . For comparison with the experiment, band-pass filtering of $G(B)$ was performed (lower curve).

The backscattering of electrons incident from the supplying quantum wires produces complex vortices inside the triangular quantum dots as can be seen from the $d\mathbf{J}(x,y)/dE$ current patterns (Fig. 6). The three-mode channel pattern is manifested in this image by regular shifts of the main $d\mathbf{J}(x,y)/dE$ current (rectangular meander) between the edges of each ring branch. Summing up $d\mathbf{J}(x,y)/dE$ over y in any vertical section x_i inside the ring yields that the resultant persistent currents J_{up} , J_{down} flowing in the top and bottom ring branches only depend on E and B , are equal in absolute value and opposite in sign. In this case $d\mathbf{J}(x,y)/$

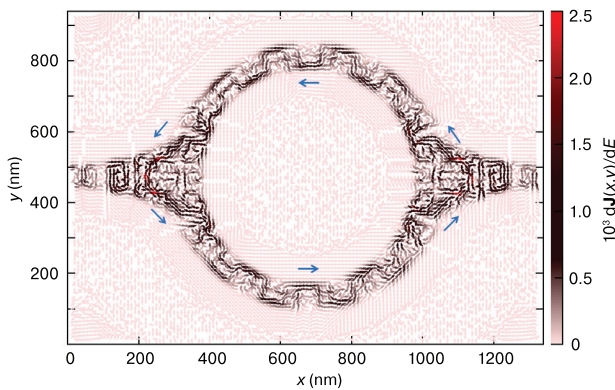


Figure 6. The contribution of $d\mathbf{J}(x,y)/dE$ to the equilibrium current for the first narrow peak dM/dE in Fig. 5 at $B = 0.0046$ T. Positive dM/dE sign corresponds to counterclockwise eddy current in the ring.

dE is shown for the first narrow $G(B)$ resonance peak. The eddy current in the ring at this B is counterclockwise.

Figure 5 shows another narrow $G(B)$ peak, i.e., a narrow dM/dE drop at $B = 0.0053$ T, near this quasisubband level. For this B the current in the $d\mathbf{J}(x,y)/dE$ plot changes to clockwise but the absolute value distribution of $d\mathbf{J}(x,y)/dE$ changes little if any (not shown) in comparison with that in Fig. 6.

Note that the total equilibrium current and magnetic moment calculations are complicated by the presence of narrow quasi-level states which may make a significant contribution and therefore the calculations should be conducted at a small step, this making them quite time-consuming, but easily parallelizable [29].

5. Conclusion

Magnetic field oscillations of conductance in nanosized systems, distributions of equilibrium (persistent) currents and magnetic moment induced by this current were calculated based on calculations results for 3D electrostatic potential in devices with ballistic quantum dots and ring interferometers. There is a correlation between the behavior of conductance and magnetic moment. Magnetic field oscillations of conductance of a quantum dot are similar to Aharonov–Bohm oscillations. The calculated period of the Aharonov–Bohm oscillations agrees with the experimental one for these devices. Since the results reported herein were obtained on the basis of experimental data on the technology and operation of mesoscopic nanosized devices [7–14], they significantly complement the former realistic simulation of quantum phenomena in solid state gate-controlled structures.

The work was supported by Grant No. 19-72-30023 of the Russian Research Foundation. Calculations involving computer resources of the Joint Supercomputer Center of the Russian Academy of Sciences were fulfilled under State Assignment No. 0306-2019-0011.

References

- Bykov A. A., Kvon Z. D., Ol'shanetskii E. B., Litvin L. V., Nastaushv Yu. V., Mansurov V. G., Migal' V. P., Moshchenko S. P., Plyukhin V. G. Quasiballistic electronic interferometer. *JETP Lett.* 1993; 57(9): 613–616.
- Persson M., Pettersson J., von Sydow B., Lindelof P. E., Kristensen A., Berggren K. F. Conductance oscillations related to the eigenenergy spectrum of a quantum dot in weak magnetic fields. *Phys. Rev. B.* 1995; 52(12): 8921–8933. <https://doi.org/10.1103/PhysRevB.52.8921>
- Micolich A. P., See A. M., Scannell B. C., Marlow C. A., Martin T. P., Pilgrim I., Hamilton A. R., Linke H., Taylor R. P. Is it the boundaries or disorder that dominates electron transport in semiconductor 'billiards'? *Fortschr. Phys.* 2013; 61(2–3): 332–347. <https://doi.org/10.1002/prop.201200081>
- Tkachenko O. A., Tkachenko V. A., Kvon Z. D., Latyshev A. V., Aseev A. L. Introspection of quantum nanoelectronic devices. *Nanotechnologies in Russia.* 2010; 5(9–10): 676–695. <https://doi.org/10.1134/S1995078010090132>
- Tkachenko V. A., Tkachenko O. A., Kvon Z. D., Latyshev A. V., Aseev A. L. Introspection in nano- and mesoscopic physics: single electronics and quantum ballistics. *Optoelectronics, instrumentation and data processing.* 2016; 52(5): 518–528. <https://doi.org/10.3103/S8756699016050149>
- Tkachenko O. A., Tkachenko V. A., Kvon Z. D., Sheglov D. V., Aseev A. L. Modeling of quantum transport and single-electron charging in GaAs/AlGaAs-nanostructures. In: *Advances in Semiconductor Nanostructures. Growth, Characterization, Properties and Applications.* Ed. by: A. V. Latyshev, A. V. Dvurechenskii, A. L. Aseev. Elsevier, 2017: 131–155. <https://doi.org/10.1016/B978-0-12-810512-2.00006-8>
- Tkachenko O. A., Tkachenko V. A., Baksheev D. G., Kvon Z. D., Portal J. C. Electrostatic potential, energy spectrum, and Fano resonances in a ballistic ring interferometer based on an AlGaAs/GaAs heterojunction. *JETP Lett.* 2000; 71(6): 255–258. <https://doi.org/10.1134/1.568328>
- Olshanetsky E. B., Cassé M., Kvon Z. D., Gusev G. M., Litvin L. V., Plotnikov A. V., Maude D. K., Portal J. C. Symmetric, gated, ballistic rings as tunable electron interferometers. *Physica E.* 2000; 6(1–4): 322–326. [https://doi.org/10.1016/S1386-9477\(99\)00160-5](https://doi.org/10.1016/S1386-9477(99)00160-5)
- Cassé M., Kvon Z. D., Gusev G. M., Olshanetsky E. B., Litvin L. V., Plotnikov A. V., Maude D. K., Portal J. C. Temperature dependence of the Aharonov–Bohm oscillations and the energy spectrum in a single-mode ballistic ring. *Phys. Rev. B.* 2000; 62(4): 2624–2629. <https://doi.org/10.1103/PhysRevB.62.2624>
- Liang C.-T., Simmons M. Y., Smith C. G., Kim G. H., Ritchie D. A., Pepper M. Experimental evidence for Coulomb charging effects in an open quantum dot at zero magnetic field. *Phys. Rev. Lett.* 1998; 81(16): 3507–3510. <https://doi.org/10.1103/PhysRevLett.81.3507>
- Liang C.-T., Simmons M. Y., Smith C. G., Kim G. H., Ritchie D. A., Pepper M. Multilayered gated lateral quantum dot devices. *Appl. Phys. Lett.* 2000; 76(9): 1134–1136. <https://doi.org/10.1063/1.125961>
- Baksheev D. G., Tkachenko O. A., Tkachenko V. A. The role of intersubband mixing in single-electron charging of open quantum dot. *Physica E: Low-dimensional Systems and Nanostructures.* 2000; 6(1–4): 414–417. [https://doi.org/10.1016/S1386-9477\(99\)00204-0](https://doi.org/10.1016/S1386-9477(99)00204-0)

13. Tkachenko O. A., Tkachenko V. A., Baksheyev D. G., Liang C.-T., Simmons M. Y., Smith C. G., Ritchie D. A., Kim Gil-Ho, Pepper M. Coulomb charging effects in an open quantum dot device. *J. Phys.: Condens. Matter*. 2001; 13(42): 9515–9534. <https://doi.org/10.1088/0953-8984/13/42/312>
14. Tkachenko V. A., Tkachenko O. A., Baksheyev D. G., Liang C.-T. Coulomb oscillations of the ballistic conductance in a quasi-one-dimensional quantum dot. *JETP Lett.* 2001; 74(4): 209–212. <https://doi.org/10.1134/1.1413551>
15. Büttiker M., Imry Y., Landauer R. Josephson behavior in small normal one-dimensional rings. *Phys. Lett. A*. 1983; 96(7): 365–367. [https://doi.org/10.1016/0375-9601\(83\)90011-7](https://doi.org/10.1016/0375-9601(83)90011-7)
16. Büttiker M. Small normal-metal loop coupled to an electron reservoir. *Phys. Rev. B*, 1985; 32(3): 1846–1849. <https://doi.org/10.1103/PhysRevB.32.1846>
17. Sivan U., Imry Y. de Haas-van Alphen and Aharonov-Bohm-type persistent current oscillations in singly connected quantum dots. *Phys. Rev. Lett.* 1988; 61(8): 1001–1004. <https://doi.org/10.1103/PhysRevLett.61.1001>
18. Jayannavar A. M., Deo P. S. Persistent currents and conductance of a metal loop connected to electron reservoirs. *Phys. Rev. B*. 1994; 49(19): 13685–13690. <https://doi.org/10.1103/PhysRevB.49.13685>
19. Fogler M. M., Levin E. I., Shklovskii B. I. Chemical potential and magnetization of a Coulomb island. *Phys. Rev. B*. 1994; 49(19): 13767–13775. <https://doi.org/10.1103/PhysRevB.49.13767>
20. Tan W.-C., Inkson J. C. Magnetization, persistent currents, and their relation in quantum rings and dots. *Phys. Rev. B*. 1999; 60(8): 5625–5635. <https://doi.org/10.1103/PhysRevB.60.5626>
21. Bremme L., Ihn T., Ensslin K. Magnetization of a two-dimensional electron gas and the role of one-dimensional edge currents. *Phys. Rev. B*. 1999; 59(11): 7305–7307. <https://doi.org/10.1103/PhysRevB.59.7305>
22. Aldea A., Moldoveanu V., Nita M., Manolescu A., Gudmundsson V., Tanatar B. Orbital magnetization of single and double quantum dots in a tight-binding model. *Phys. Rev. B*. 2003; 67(3): 035324 (10pp). <https://doi.org/10.1103/PhysRevB.67.035324>
23. Maily D., Chapelier C., Benoit A. Experimental observation of persistent currents in a GaAs-AlGaAs single loop. *Phys. Rev. Lett.*, 1993; 70(13): 2020–2023. <https://doi.org/10.1103/PhysRevLett.70.2020>
24. Rabaud W., Saminadayar L., Maily D., Hasselbach K., Benoot A., Etienne B. Persistent Currents in mesoscopic connected rings. *Phys. Rev. Lett.* 2001; 86(14): 3124–3127. <https://doi.org/10.1103/PhysRevLett.86.3124>
25. Schwarz M. P., Grundler D., Wilde M. A., Heyn Ch., Heitmann D. Magnetization of semiconductor quantum dots. *J. Appl. Phys.* 2002; 91(10): 6875–6877. <https://doi.org/10.1063/1.1450762>
26. Schwarz M. P., Wilde M. A., Groth S., Grundler D., Heyn Ch., Heitmann D. Sawtoothlike de Haas-van Alphen oscillations of a two-dimensional electron system. *Phys. Rev. B*. 2002; 65(24): 245315 (9pp). <https://doi.org/10.1103/PhysRevB.65.245315>
27. Usher A., Elliott M. Magnetometry of low-dimensional electron and hole systems. *J. Phys.: Condens. Matter*. 2009; 21: 103202 (31pp). <https://doi.org/10.1088/0953-8984/21/10/103202>
28. Cresti A., Farchioni R., Grosso G., Parravicini G. P. Keldysh-Green function formalism for current profiles in mesoscopic systems. *Phys. Rev. B*. 2003; 68(7): 075306 (8pp.). <https://doi.org/10.1103/PhysRevB.68.075306>
29. Tkachenko O. A., Tkachenko V. A. Supercomputer modeling of semiconductor quantum nanosystems. *Vychislitel'nyye metody i programirovaniye = Numerical methods and programming*. 2012; 13(1): 253–262. (In Russ.)